JOURNAL OF Applied Polymer SCIENCE

Rheological, Thermal, and Mechanical Properties of P (3HB-*co*-4HB) and P (3HB-*co*-4HB)/EVA Blends

Jing Guo,[1,2] Mengzhu Liu,[1] Yuanfa Liu,[1] Chengnv Hu,[1] Ying Xia,[1] Hong Zhang,[1] Yumei Gong[1]

[1]School of Textile and Material Engineering, Dalian Polytechnic University, Dalian 116034, People's Republic of China

[2]Liaoning Engineering Technology Research Centre of Function Fiber and its Composites, Dalian Polytechnic University, Dalian 116034, People's Republic of China

Correspondence to: J. Guo (E-mail: guojing8161@163.com)

ABSTRACT: Poly(3-hydroxybutyrate-*co*-4-hydroxybutyrate) [P(3HB-*co*-4HB)] fiber and P(3HB-*co*-4HB)/EVA fiber were obtained by single screw extrusion machine. The rheology of P(3HB-*co*-4HB) and P(3HB-*co*-4HB)/EVA blends was characterized by capillary rheometer, and the chemical groups of the blends were characterized with Fourier transform infrared spectroscopy (FT-IR). The crystallization behavior and thermal, mechanical and elastic properties of the fibers were measured by differential scanning calorimeter (DSC), thermogravimetric analyzer (TGA) and single fiber strength tester, respectively. Besides, the moisture regain and drying shrinkage rates of the fibers were tested. These results showed that P(3HB-*co*-4HB)/EVA blends have better flowability, crystallinity, and thermal stability than P(3HB-*co*-4HB) fiber. The fracture strength of the P(3HB-*co*-4HB)/EVA fiber decreases with increasing the EVA content, but the elongation at break shows the contrary tendency. The rebound resilience ratio of P(3HB-*co*-4HB)/EVA fiber reaches 100%. Both moisture regain and drying shrinkage increase first and then decrease with increasing the EVA content. © 2014 Wiley Periodicals, Inc. J. Appl. Polym. Sci. **2014**, *131*, 41206.

KEYWORDS: composites; fibers; rheology; thermal properties

Received 29 March 2014; accepted 22 June 2014

DOI: 10.1002/app.41206

INTRODUCTION

Because the world oil reserve is dwindling, oil price rises continuously, the global energy crisis is getting worse, environmental pollution has become more and more serious, and many countries have limited the applications of synthetic polymer materials. Therefore, the biodegradable polymer materials are receiving people's great attention. Among these materials, polyhydroxyalkanoates (PHAs) are a type of intracellular polyester synthesized by many prokaryotic microbes in the unbalanced growth conditions (such as excess carbon source, insufficient nitrogen, phosphorus, magnesium or oxygen, and other insufficient nutrition conditions). PHAs are promising materials for biomedical Engineering, car, electronics, coating and textile applications because they are biodegradable, non-toxic and biocompatible.[1] Poly 3-hydroxybutyrate-*co*-4-hydroxybutyrate [P(3HB-*co*-4HB)] is the fourth generation of PHA products. Chanprateep et al., produced P(3HB-*co*-4HB) by Cupriavidus necator strain A-04, and then P(3HB-*co*-4HB) with a 0, 5, 24, 38, and 64% mole fraction of 4HB content were purified and prepared as plastic films.[2] The mechanical properties and biocompatibility of these films were tested and compared with commercial PHB, polystyrene (PS), and polyvinylchloride (PVC) prepared without additives. The results demonstrated that PHB had thermal and mechanical properties similar to those of commercial PHB. The P(3HB-*co*-4HB) polymers possessed melting temperature and glass transition temperature values higher than those reported previously. The mechanical properties were compared with those of PS and PVC. P(3HB-*co*-4HB) films have good surface characteristics and can promote cell attachment, proliferation and differentiation. Guo et al. investigated the rheological and thermal properties and crystallinity of P (3HB-co-4HB) by RH2000 capillary rheometer, DSC, TGA, polarizing optical microscope (POM). The results showed that P(3HB-*co*-4HB) melt is typical pseudo plastic fluid, its glass-transition temperature is minus 10°C, the melting temperature is between 100 and 120°C, the decomposing temperature is 205°C, and the maximum radial growth rate temperature of P (3HB-*co*-4HB) spherocrystal appears at about 78°C.[3] Zhang et al. prepared P(3HB-*co*-4HB) films by uniaxial cold-drawing from an amorphous preform at the glass transition temperature and investigated the molecular and highly ordered structures and physical properties of cold-drawn films. The results showed tensile strength, elongation to break and

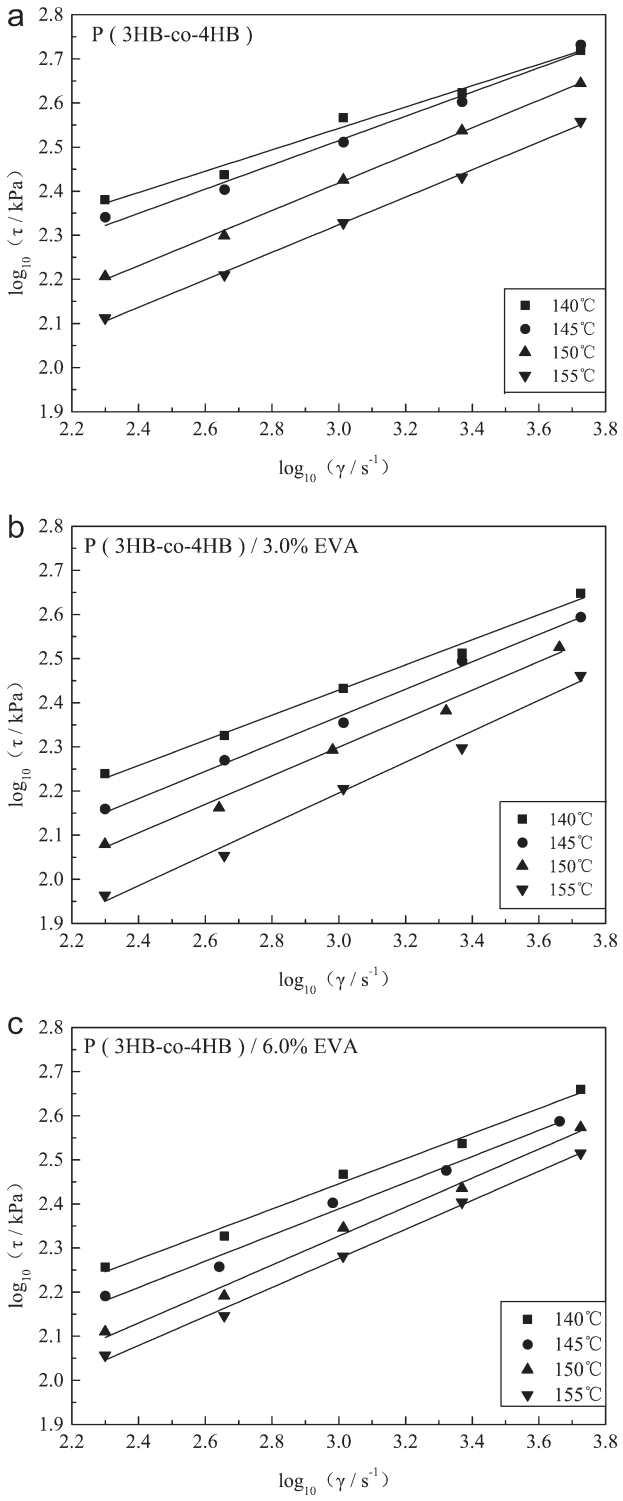

Figure 1. lg $\tau\sim$ lg γ relationship of P (3HB-*co*-4HB) and P (3HB-*co*-4HB)/EVA melt.

Young's modulus of P(3HB-*co*-4HB) with cold-drawn ratio 1200% reached 290 MPa, 58% and 2.8 GPa, respectively.[4] The enzymatic degradation rate increased with increasing draw ratio, and increased greatly with increasing 4HB content. However, until now there is no commercial application of P (3HB-*co*-4HB) in large scale due to its narrow processability window and slow crystallization speed. These drawbacks of P(3HB-*co*-4HB) can be overcome by blending other polymer to improve processability and reduce brittleness. Weng et al. reported that P(3HB-*co*-4HB)/PLA blends can be used to prepare biodegradable polymeric materials with good comprehensive properties, it can be biodegraded under real soil conditions, and has different degradation rates in different depths of soil.[5] Wang prepared blend films of poly(3-hydroxybutyrate-*co*−3-hydroxyvalerate) (PHBV)/P(3HB-*co*-4HB) by solvent-cast method. The nonisothermal crystallization results shows that PHBV and P(3 HB-*co*-4HB) are miscible due to a single glass transition temperature (T_g), which is dependent on blend composition. The isothermal crystallization results demonstrate that the crystallization rate of PHBV becomes slower after adding amorphous P(3HB-*co*-4HB), which could be proved through depression of equilibrium melt point (equation image) from 183.7 to 177.6°C. PHBV and PHBV/P(3HB-*co*-4HB) blend, the maximum crystallization rate appeared at 88 and 84°C, respectively. Meanwhile, PHBV is changed to ductile materials by addition of P(3HB-*co*-4HB).[6] Guo et al. showed that the thermal stability of P(3HB-co-4HB)/PEG10000 blends was better than that of that P(3HB-*co*-4HB).[7] The non-Newtonian index *n* of the P(3HB-*co*-4HB)/PEG10000 blends increases and its flow activation energy decreases. Wang et al. showed that polyhedral oligomeric silsesquioxane (POSS) acted as nucleating agents. At low concentrations (1%), POSS can increase crystallization temperature and mechanical properties of blends.[8] The nucleating effect improves as POSS fraction increases, but thermal stability and mechanical properties decrease due to the worse dispersion of POSS.

At present, there is relatively little research about modification and processing forming or applications of P(3HB-*co*-4HB) fiber. And right now the mainly used spinning methods are electrostatic spinning[9] and melt spinning.[10] In this research, these fibers with excellent performance were obtained successfully via melt spinning, by blending EVA (ethylene-vinyl acetate) with P(3HB-*co*-4HB).

EXPERIMENTAL

Experiment Materials

P (3HB-*co*-4HB), whose number-average molecular weight is about 700,000, and 4HB molar percentage is 15%, was supplied by Shenzhen Italian Man Biotechnology. It was dried at 95°C for 24 h in a vacuum oven before spinning. Ethylene-vinyl acetate (EVA) copolymer, whose grade is P2805, VAC content is 28%, and melt index is 6, was supplied by Mitsui Chemical.

Table I. Non-Newtonian Index *n* of P (3HB-*co*-4HB) and P (3HB-*co*-4HB)/EVA Melt

	Non-Newtonian index n			
P(3HB-*co*-4HB)/ EVA mass ratio	140°C	145°C	150°C	155°C
100/0	0.242	0.275	0.313	0.313
97/3	0.282	0.312	0.328	0.348
94/6	0.285	0.297	0.328	0.329

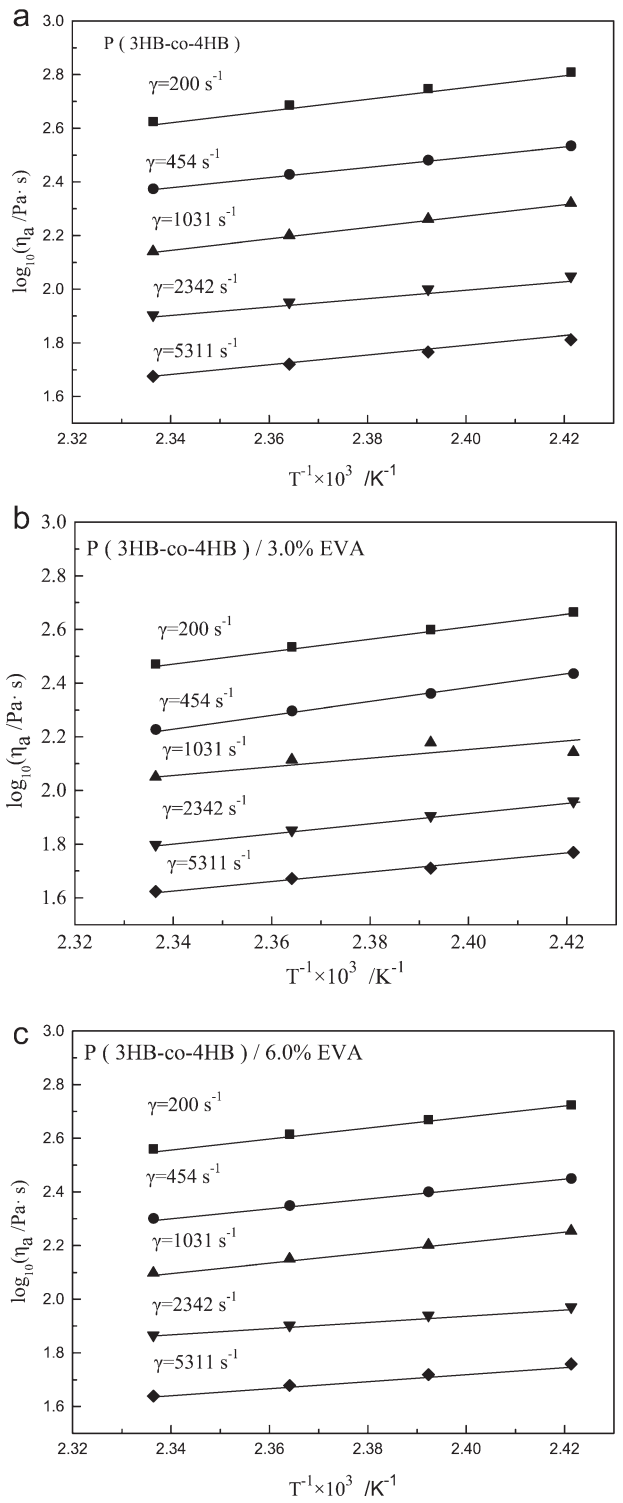

Figure 2. ln $\eta_a \sim T^{-1}$ relationship of P (3HB-*co*-4HB) and P (3HB-*co*-4HB)/EVA melt.

Preparation of P(3HB-*co*-4HB)/EVA Fiber

P(3HB-*co*-4HB)/EVA spun fiber was prepared by a single screw extrusion machine under the following conditions: melt spinning temperature range of 125–150°C, screw speed of 30 r min^{-1}, spinneret of 18 holes, the nozzle diameter of 0.22 mm, the nozzle length of 0.55 mm. The spun fiber was drawn 400% in hot air at 80°C ± 5°C.

Test and Characterization

Rheological Properties. The rheological properties of P(3HB-*co*-4HB)/EVA systems were tested by a RH2000 type capillary rheometer manufactured by British Rosand. Capillary diameter was 0.5 mm, aspect ratio was 16 : 1, shear rates were 200–10,000 s^{-1}, and temperatures were 140, 145, 150, and 155°C.

DSC. Swiss Mettler DSC-2C differential scanning calorimeter (DSC) was used. Heating rate was 10°C min^{-1} and scanning temperature range is between −60°C and 165°C.

TGA. Thermogravimetric analyzer (TGA) Q50 TA analyzer was used. Heating rate was 20°C min^{-1}, scanning temperature range was from room temperature to 700°C, and flow atmosphere was under the high purity nitrogen at 50 mL min^{-1}.

FT-IR. Porphyrized P(3HB-*co*-4HB), EVA and P(3HB-*co*-4HB)/EVA fibers were prepared with KBr press method and tested by the Spectrum One-B Fourier transform infrared Spectrum analyzer FT-IR.

Mechanical Properties and Rebound Resilience. They were tested by a monofilament strength tester purchased from Laizhou Electronic Instrument Limited Company under the following experimental conditions: temperature of 20°C, humidity of 65%, tensile speed of 20 mm min^{-1}, chuck gauge of 10 mm. Each sample was repeated 20 times to take the average. Rebound resilience was tested under the elasticity of constant elongation: 50, 100, and 150%, respectively. Moisture regain: A dry weight, M_1, was gained after random samples were dried in an oven to a constant weight, and then another weight, M_2, was gained after the samples were kept at 20°C and 65% relative humidity for 24 h. Moisture regain is calculated by the following equation.

$$\text{Moisture regain} = (M_2 - M_1)/M_1 \times 100\% \quad (1)$$

Dry Shrinkage Rate. First, 0.3 g load was hung below the fiber to make it straight but not stretched, and then the original length, about 500 mm, of the fiber was recorded as l_0. Second, the fiber was folded and placed in a oven at 100°C for 30 min. Then, the fiber was removed out and cooled down to room temperature. Finally, the load was re-hung, and the final length was recorded as l_1. Dry Shrinkage rate is calculated by eq. (2).

$$\text{Dry shrinkage rate} = (l_1 - l_0)/l_0 \times 100\% \quad (2)$$

RESULTS AND DISCUSSION

Rheological Properties

Relationship Between Shear Stress and the Apparent Shear Rate. Figure 1 is curves of the apparent shear stress (τ) vs. the apparent shear rate (γ) for P(3HB-*co*-4HB) and P(3HB-*co*-4HB)/EVA melt at different temperatures. Figure 1 shows that the denary logarithm τ and denary logarithm γ curves of the P(3HB-*co*-4HB) and P(3HB-*co*-4HB)/EVA melt are nearly in a linear relationship, which is accorded with the Ostwald–de Wale power law, The linear slopes, the non-Newtonian index, n, of materials, are shown in Table I. It can be seen that P(3HB-*co*-4HB) and P(3HB-*co*-4HB)/EVA blends melt are typical

Table II. Viscous Flow Activation Energy of P(3HB-*co*-4HB)/EVA Composites with Different Mass Ratio

P(3HB-*co*-4HB)/EVA mass ratio	$\triangle E_\eta$/ kJ mol^{-1}				
	200 s^{-1}	454 s^{-1}	1031 s^{-1}	2342 s^{-1}	5311 s^{-1}
100/0	41.63	39.52	40.65	32.76	30.68
97/3	43.60	46.71	43.40	36.31	32.87
94/6	36.97	35.43	35.54	27.09	25.18

pseudoplastic fluid, whose values of n are <1 and increases with temperature. It is because the macromolecular chain segments have higher energy and more free volume at a higher melting temperature. The macromolecules have enough energy and space to achieve the full relaxation of molecular chain and melt flow resistance is small, so the values of n increases. In Table I, we can also see that n values of blends melt are higher than those of pure P(3HB-*co*-4HB) melt at the same temperature due to the reduced intermolecular entanglement .The n value of P(3HB-*co*-4HB)/EVA blends at EVA content of 3% reaches a maximum.

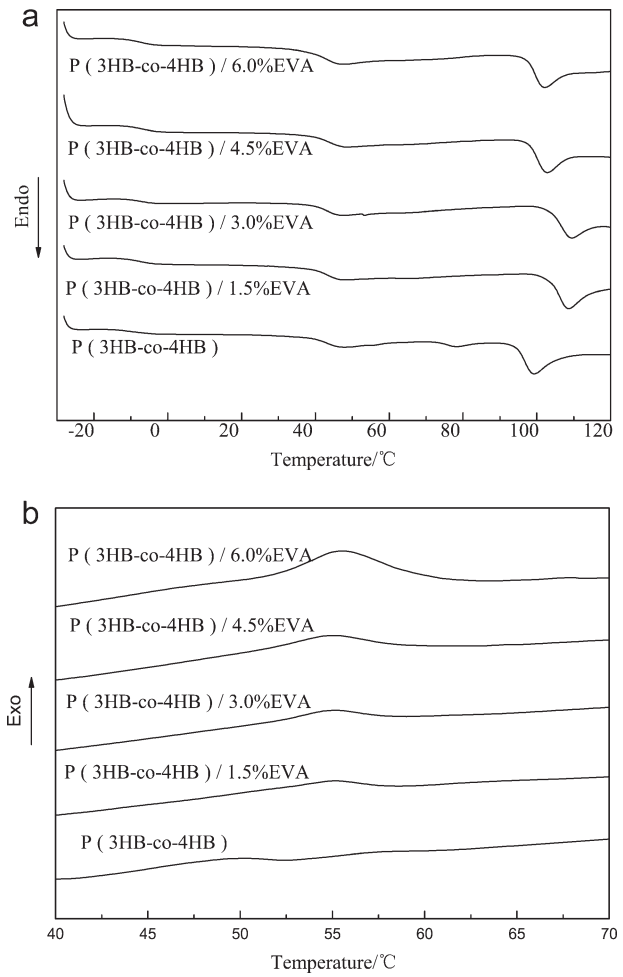

Figure 3. DSC curves of P (3HB-*co*-4HB)/EVA. (a): the melting endothermic curves,(b) the crystallization exotherm curves).

Relationship Between Apparent Shear Viscosity and Temperature. As shown in Figure 2, the apparent shear viscosity of P(3HB-*co*-4HB) and P(3HB-*co*-4HB)/EVA melt decreases with increasing shear rate at the same temperature. When the shear rate increases, disentanglement between the macromolecular chains occurs, the intermolecular entanglement points reduces, and the intermolecular interaction force decreases, thereby reducing the flow resistance of melt.

Figure 2 shows the linear relationship between the natural logarithm of apparent shear viscosity (η_a) and the reciprocal of temperature (T^{-1}), which can be described by Arrhrnius equation:

$$\eta_a = A \exp\ (E_\eta/\mathrm{RT}) \qquad (3)$$

where A is constant, R is molar gas constant and E_η is viscous flow activation energy. According to the straight slope of Figure 2, the viscous flow activation energy, E_η, of P(3HB-*co*-4HB) and P(3HB-*co*-4HB)/EVA melt can be obtained, as shown in Table II. It can be seen that the viscous flow activation energy decreases with the increase of shear rate, indicating that the sensitivity of the apparent shear viscosity to temperature is highly dependent on the shear rate. Under lower shear rate, the apparent shear viscosity largely decreases with increase of temperature. Under higher shear rate, the apparent shear viscosity slightly diminishes with increasing temperature. From Table II it can be seen that the viscous flow activation energy values are the highest when P(3HB-*co*-4HB)/EVA mass ratio is 97/3, and the values are the lowest at the ratio of 94/6. When EVA content is small, EVA and P(3HB-*co*-4HB) macromolecules form intermolecular physical entanglement, and constitute physical entanglement network, which makes melt flow worse and viscous flow activation energy increase. However, when EVA content continuously increase, part of the excess EVA molecules do not form intermolecular physical entanglement with P(3HB-*co*-4HB) molecules, and they are free in the flow layers acting as a plasticizer, which makes the macromolecular interlayer glide

Table III. T_g and T_m of P(3HB-*co*-4HB)/EVA

P(3HB-*co*-4HB)/ EVA mass ratio	T_g of 4HB segments (°C)	T_g of 3HB segments (°C)	T_m (°C)
100/0	−8.47	43.20	99.17
100/1.5	−7.68	43.28	108.50
100/3.0	−7.31	43.21	109.04
100/4.5	−6.54	43.54	102.52
100/6.0	−7.73	43.30	101.99

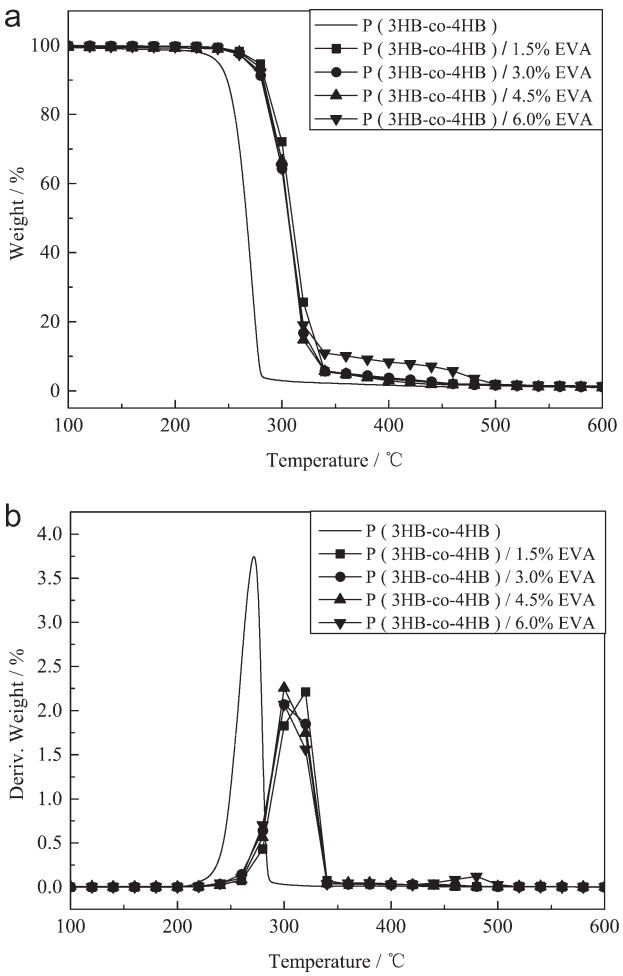

Figure 4. TG and DTG cures of P(3HB-*co*-4HB)/EVA composites.

much easier, thereby reducing the viscous flow activation energy.

DSC

In Figure 3(a), we can see three peaks, which are corresponding to the glass transition temperature (T_g) of 4HB and 3HB segment, and the melting points T_m of the blends. The thermal properties by DSC are listed in Table III. It can be seen that T_g and T_m of P(3HB-*co*-4HB/EVA blends are higher than those of pure P(3HB-*co*-4HB) and EVA. T_m first increases and then decreases with increasing the content of EVA, and reaches the maximum value of 109.04°C at EVA content of 3%. The physical entanglement between EVA and P(3HB-*co*-4HB) macromolecules leads to a formation of three dimensional crosslinked network structure, so the density of entanglement points increases with EVA content. However, when EVA is excessive, the free EVA in the intermolecular plays a role as plasticizer, which makes the melting points of materials reduce. When EVA content increases, the T_g of 4HB segment first increases and then decreases, and T_g of 3HB segment has no obvious change, indicating that the physical entanglement mentioned above occurs in 4HB segment.

In Figure 3(b), pure P(3HB-*co*-4HB) has a blunt crystallization peak at about 50°C. However, P(3HB-*co*-4HB)/EVA blends has a relative sharp crystallization peak at around 55°C, and their peak areas increase with increasing EVA content. These results indicate that EVA can improve the crystallization temperature and crystallinity of fibers. As we know, in the absence of a seed, spontaneous fluctuation is needed to form a crystal nucleus that exceeds the critical size. However, crystallization can proceed spontaneously if we add a seed crystal that is larger than the critical nucleus to the metastable liquid phase. The three dimensional crosslinked network structure between EVA and P(3HB-*co*-4HB) mentioned above act as a role of seed crystal.

TGA

In Figure 4, TG and DTG (derivative thermogravimetric analysis) curves show that the outset decomposition temperature, maximum decomposition temperature and end decomposition temperature of P(3HB-*co*-4HB)/EVA fiber are higher (+40°C) than those of P(3HB-*co*-4HB) fiber. It indicates that the addition of EVA can significantly improve thermal stability performance of P(3HB-*co*-4HB) fiber In Table IV, it can be seen clearly that $T_{5\%}$, $T_{50\%}$, $T_{95\%}$, and T_{max} ($T_{5\%}$, $T_{50\%}$, $T_{95\%}$, and T_{max} express the corresponding temperature of weight loss: 5, 50, 95% and maximum, respectively) of the P(3HB-*co*-4HB)/EVA fiber are higher than those of pure P(3HB-*co*-4HB) fiber. As shown in DSC results, the crystallinity of P(3HB-*co*-4HB)/EVA fiber is improved with the increasing EVA content, because the entanglement effect between EVA and P(3HB-*co*-4HB) molecules makes the materials need a higher temperature to be degraded.

FT-IR

The FT-IR diagram for P(3HB-*co*-4HB) fibers, before and after modified by EVA, is shown in Figure 5, where three spectrum curves all have a strong absorption peak at 3435 cm^{-1}, which may be caused by the intermolecular hydrogen bond. The absorption peak at 2921.66 and 2851.51 cm^{-1} is symmetric and antisymmetric stretching vibration peak of —CH2—. And the peak vibration of P(3HB-*co*-4HB)/EVA spectrums is strengthened compared with P(3HB-*co*-4HB), as —CH2— content increases. The absorption peak at 1725.87 cm^{-1} is stretching vibration peak of —C═O—, and the vibration peak is obviously stronger than P(3HB-*co*-4HB) spectrum curve, as the —C═O— content increase, indicating that the modification are effective. Spectrum curves of P(3HB-*co*-4HB)/EVA fiber and EVA have several continuous absorption peaks at 900–500 cm^{-1},

Table IV. Weight Loss Temperatures of P (3HB-*co*-4HB) and P (3HB-*co*-4HB)/EVA Composite

P(3HB-co-4HB)/ EVA mass ratio	$T_{5\%}$ (°C)	$T_{50\%}$ (°C)	$T_{95\%}$ (°C)	T_{max} (°C)
100/0	240.5	266.9	280.3	271.6
100/1.5	279.0	310.3	353.5	313.5
100/3.0	272.4	306.2	363.0	310.0
100/4.5	276.9	306.4	356.0	309.5
100/6.0	275.0	306.1	467.7	309.0

Note: In Table IV, $T_{5\%}$, $T_{50\%}$, $T_{95\%}$, and T_{max} express the corresponding temperature of weight loss: 5, 50, 95% and maximum, respectively.

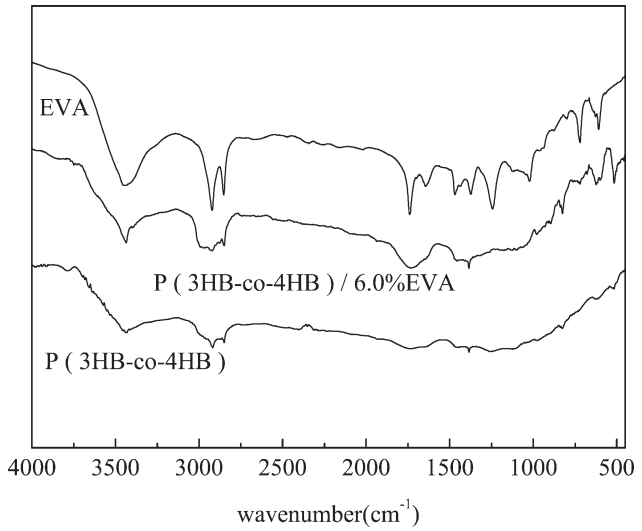

Figure 5. FT-IR figure of P (3HB-*co*-4HB), EVA and P (3HB-*co*-4HB)/EVA.

corresponding to the fingerprint region characteristic peak of EVA. However, the peak position for two polymers is not simple superposition, indicating the intermolecular interactions of fiber occur.

Mechanical Properties

In Table V, the fracture strength of the P(3HB-*co*-4HB)/EVA fibers (drawn 400%) reduces with increasing of EVA content. The higher EVA content, the more polar group —COO— in the systems. The intermolecular space steric hindrance increases and the intermolecular distance increases, but the intermolecular force reduces, thereby reducing the fibers' fracture strength. Besides, the higher the EVA content, the bigger the gap between EVA and matrix P(3HB-*co*-4HB), the lower the interface strength, the more vulnerable to occur the stress concentration. So the fracture strength of fiber is lower. In Table V, elongation at break of P(3HB-*co*-4HB)/EVA fiber is higher than that of P(3HB-*co*-4HB) fiber. The elongation at break of P(3HB-*co*-4HB)/EVA fiber increases with EVA content, and reaches the maximum of 304.28% at EVA content of 6% owing to the entanglement network between EVA and P(3HB-*co*-4HB) molecules.

Rebound Resilience

In Figure 6, we can clearly see that rebound resilience ratio of the P(3HB-*co*-4HB) fiber is 83.42, 74.48, and 67.53% for

Table V. EVA Content and Mechanical Properties of Fibers

P(3HB-co-4HB)/EVA mass ratio	Fracture strength / (cN/dtex)	Elongation at break (%)
100/0	1.68	152.96
100/1.5	1.58	200.87
100/3.0	1.26	240.65
100/4.5	1.18	248.58
100/6.0	0.77	304.28

Note: The draw ratio is 400%.

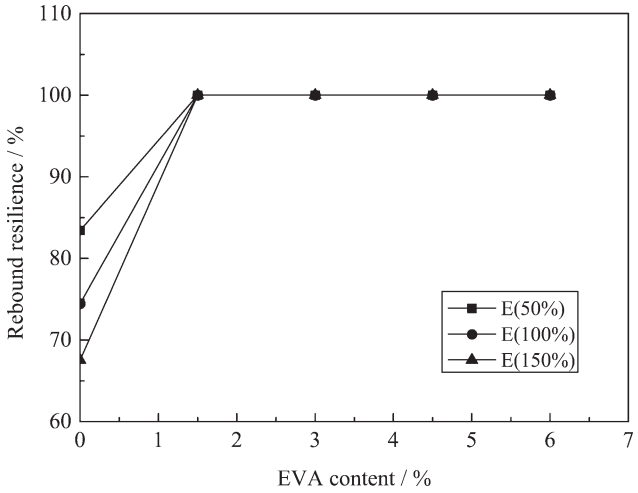

Figure 6. The relationship of EVA content and fiber elastic recovery rate.

E(50%), E(100%), and E(150%), respectively. While the rebound resilience ratio of all P(3HB-*co*-4HB)/EVA fibers are 100% regardless of the elongation elasticity, suggesting that EVA can significantly improve the resilience of P(3HB-*co*-4HB) fiber. Resilience of fiber depends on the macromolecular conformation, the ordering degree of aggregation state, and especially the aggregation state structure in amorphous area. After adding EVA, preferential arrangement degree of macromolecular chain increases axially in fibers' amorphous area, the orientation degree enhances, and ordering degree of aggregation state increases. Therefore, the resilience of fiber is largely improved.

Moisture Regain

In Figure 7, the moisture regain of the P(3HB-*co*-4HB)/EVA fiber first increases and then decreases with increasing of EVA content, and reaches a maximum of 0.33% at EVA content of 1.5%, which is 136% of that of pure P(3HB-*co*-4HB) fiber. It is mainly due to the intermolecular entanglement between EVA and P(3HB-*co*-4HB) molecules and the constituted crosslinking network where the water can enter. Furthermore, after adding EVA, the phase interface void and specific surface area increase, so moisture regain increases. However, it should be noted that

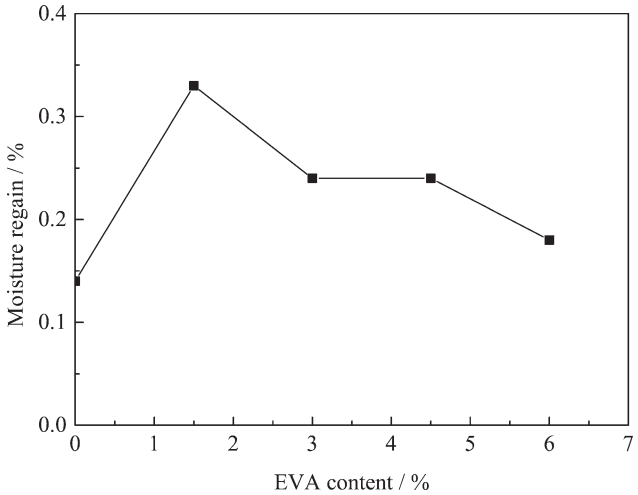

Figure 7. The relationship of EVA content and fiber moisture regain.

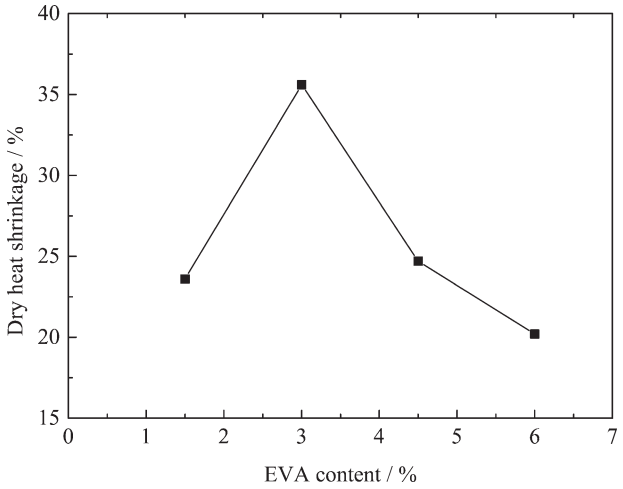

Figure 8. The relationship of EVA content and fiber dry heat shrinkage.

EVA is a hydrophobic polymer. The more the EVA added, the higher the hydrophobicity of fiber. Therefore, the moisture regain of fibers reduces when the EVA content is >1.5%.

Dry Heat Shrinkage

In Figure 8, dry heat shrinkage rates of P(3HB-*co*-4HB)/EVA fiber first increase then decrease with increasing of EVA content, and reach a maximum of 35.6% at EVA content of 3%. As mentioned previously, as the EVA content increases, the crystallinity of fiber is improved, the amorphous area is reduced and ordering degree of macromolecules is increased. As a result, the shrinkage of fiber is declined. On the other hand, because intermolecular entanglement between EVA and P(3HB-*co*-4HB) occurs, disordering degree of fibers increases, the disorientation increases, and the shrinkage rate rises. At low EVA content, the crystallinity of fiber is slightly improved, so the intermolecular entanglement is the dominant factor. However, with continuously increasing EVA content, the crystallization factor dominates gradually. As a result, the shrinkage of fiber first increases and then decreases with EVA content.

CONCLUSIONS

Based on rheological analysis, it can be concluded that P(3HB-*co*-4HB) and P(3HB-*co*-4HB)/EVA melts are typical pseudoplastic fluids. When temperature and shear rate increase, the apparent viscosity of the P(3HB-*co*-4HB)/EVA melts reduces, and the n value increases. DSC and TGA analyses show that crystallization temperature, crystallinity, and thermal stability of P(3HB-*co*-4HB)/EVA blends increase as temperature and shear rate increase. FT-IR shows that there is an intermolecular interactions of fiber between EVA and P(3HB-*co*-4HB). With increasing of EVA content, fibers' fracture strength decreases, but the break elongation increases. The rebound resilience ratio of P(3HB-*co*-4HB)/EVA fiber reaches 100%, which is much higher that of P(3HB-*co*-4HB) fiber. The moisture regain of P(3HB-*co*-4HB)/EVA fiber first increases and then decreases with increasing of the EVA content, and reaches a maximum of 0.33% at the EVA content of 1.5%. Dry heat shrinkage rates of the P(3HB-*co*-4HB)/EVA fibers increase first and then decrease along with increasing of EVA content and reaches a maximum of 35. 6% at EVA content of 3%.

ACKNOWLEDGMENTS

The project was funded by education department of general item, personnel support program project of Liaoning province (No: LR2012017) and The National Natural Science Foundation of China (No: 51373027) and State Key Laboratory for Modification of Chemical Fibers and Polymer Materials, Dong Hua University (v201106).

REFERENCES

1. Suffian, M. A.; Thorsten, H. *J. Appl. Polym. Sci.* **2013**, *129*, 3079.
2. Chanprateep, S.; Buasri, K.; Muangwong, A.; Utiswannakul, P. *Polym. Degrad. Stabil.* **2010**, *95*, 2003.
3. Guo, J.; Xiang, H. X.; Zhen, N.; Wang, Q. Q. *China Synth. Resin Plast.* **2011**, *28*, 52.
4. Zhang, J. Q.; Kasuya, K.; Hikima, T.; Takata, M.; Takemuraa, A.; Iwata, T. *Polym. Degrad. Stabil.* **2011**, *96*, 2130.
5. Weng, Y. X.; Wang, L.; Zhang, M.; Wang, X. L.; Wang, Y. Z. *Polym. Test.* **2013**, *32*, 60.
6. Wang, X. J.; Chen, Z. F.; Chen, X. Y.; Pan, J. Y.; Xu, K. T. *J. Appl. Polym. Sci.*, **2010**, *117*, 838.
7. Guo, J.; Zheng, N.; Zhang, S. N. *Mater. Adv. Mater.* **2011**, *152–153*, 1611.
8. H. S.; Cong, C. B.; Du, W. J.; Xu, R. W.; Yu, D. S. *Polym. Mater. Sci. Eng.* **2009**, *25*, 128.
9. He, T. T.; Tao, D.; Wei, Q. F.; Wang, Q. Q.; Zou, J. L. *China Synth. Fiber Indus.* **2011**, *34*, 5.
10. Guo, J.; Hu, C. N.; Zhang, X.; Li, X. C.; Zha, J.; Guan, F. C. *AATCC Rev.* **2013**, *13*, 50.